3

Amorphous Nanosilica Mediates Cellular Toxicity and Inflammation *via* the Inflammasome Adapter Protein ASC

3.1 ABSTRACT

Nanoparticles are small-scaled multi-functional carrier platforms for absolute manipulation of physical, chemical and biological processes. The unique physico-chemical properties of nanoparticles make them indispensable for a variety of industrial and biomedical applications. Nanoparticles can easily invade our skin, vital organs, blood vessels, and even surpass the blood-brain barrier. Once internalized, the unintended interactions between nanoparticles and complex biological systems trigger inadvertant immune and cytotoxic responses. This unconventional cellular and molecular signaling may contribute to greater suceptibilty towards infections, several auto-immune disorders and inflammation-associated diseases including cancer. Amorphous nanosilica, considered to be biologically inert is immensely popular as targeted-drug delivery systems. In the last decade, amorphous nanosilica has exhibited an exponential increase in applications, related to agriculture, food packaging, textiles, cosmetics and biomedicine. Nanosilica profoundly affects humans through various environmental and commercial sources. Despite the widespread use of amorphous nanosilica, the long term effects, cellular and molecular mechanisms there of and temporal regulation remain largely unexplored. Our study analyzes size, concentration and exposure time-dependent effects of amorphous nanosilica on human bronchoalveolar epithelial, endothelial and fibroblast cells (figure 3.1). Additionally, we have investigated innate immune regulators associated with nanosilica internalization and subsequently activated inflammation-associated pathways. The results reveal distinct nanosilica-induced cytotoxity for each cell type. Nanosilica uptake is actin cytoskeleton dependent in large size (22nm) and independent for smaller size particles(12nm). Additionally, we found that the inflammasome adaptor protein, ASC shows nuclear localization following nanosilica exposure. Moreover, ASC expression and speck formation increases in response to 12 nm nanosilica. Our results highlight possible temporal regulation of nanosilica uptake and the cellular and molecular mechanisms of nanosilica induced inflammation and cell death in human lung cell population.

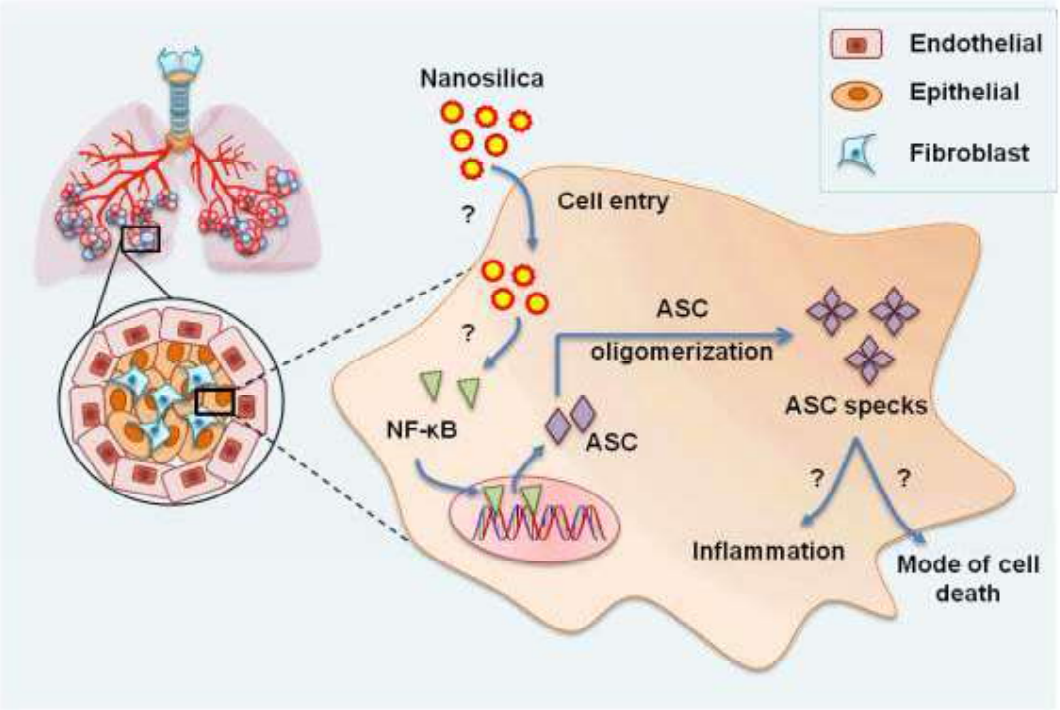

Figure 3.1 : *Amorphous nanosilica induces ASC-mediated inflammation in human lung cell population.* Amorphous nanosilica provides a highly dynamic multifunctional platform implicated in various industrial and biomedical applications. Our study aims to provide insights into cellular and molecular effects of nanosilica exposure in humans. We have analyzed size, concentration and time-dependent effects of amorphous nanosilica in human bronchoalveolar epithelial, endothelial and fibroblast cells. Apoptosis-associated CARD containing speck-like protein (ASC) is central to several inflammation and cell death-associated pathways. Therefore, we also explored the expression, activation and cellular localization of ASC in response to amorphous nanosilica exposure. Additionally, cellular pathways associated with nanosilica internalization and subsequent cell death, were also elucidated.

3.2 INTRODUCTION

Silica, a group of minerals composed of two most abundant elements, silicon and oxygen, occurs in both crystalline and amorphous forms [Napierska, Thomassen *et al.*, 2010]. Until recently, toxicological studies focused on the association of crystalline silica exposure with fibrotic lung disease (pneumoconiosis), lung cancer, chronic obstructive pulmonary disease and pulmonary tuberculosis. As amorphous silica is considered to be safer than crystalline silica, it is used widely in pharmaceutical products, paints, cosmetics, and food. Moreover, with the development of nanotechnology, practical uses for amorphous silica nanoparticles (<100 nm diameter particles) are rapidly expanding owing to its unique physicochemical properties {Moghimi, 2005 #1404; Slowing, 2007 #1405; Hirsch, 2003 #1403; Vijayanathan, 2002 #1406; Bowman, 2010 #1402}. Also, nanosilica is used in a variety of biomedical applications such as cancer therapeutics, drug delivery and enzyme immobilization 3-6. While several studies have confirmed the toxicity of amorphous and crystalline silica *in vivo* and *in vitro* {Cho, 2007 #1408; Kaewamatawong, 2005 #1407}, the toxicity of nanosilica particles continue to be controversial {Morishige, 2010 #1409; Waters, 2008 #1411; Morishige, 2012 #1410}. The majority of studies

have focused on sizes of nanosilica that show bulk properties (typically larger than 30nm){Auffan, 2009 #1412}. Nanoparticles are routinely defined as particles with sizes between about 1 and 100 nm that show properties that are not found in bulk samples of the same material. In this study, we analyze size, concentration and exposure time-dependent effects of two sizes (12nm and 22nm) of monodisperse colloidal amorphous nanosilica on human bronchoalveolar epithelial, endothelial, fibroblast and innate immune cell lines to gain mechanistic insights into interactions at the nano-bio interface in different cell lines.

One of the mechanisms by which the innate immune system differentiates between "self" from "non-self" is the highly specific, germline-encoded PRRs. NLRs are the most studied and specialized class of PRRs. NLRs respond to damage and pathogen associated molecular patterns as well as exogenous foreign particulates such as silica. Upon activation several NLRs form large multiprotein assembly called "inflammasomes". Inflammasomes consist of an NLR, an adapter molecule, ASC (apoptosis-associated speck-like protein containing a CARD [caspase recruitment domain]) and an inflammatory protease procaspase-1 [Franchi, Eigenbrod *et al.*, 2009]. ASC is critical for recruitment of pro-caspase-1 *via* homotypic CARD-CARD interactions [Srinivasula, 2002]. Procaspase-1 undergoes autoproteolytic cleavage in the inflammasome complex to form mature active Caspase-1. Activated Caspase-1 in turn cleaves and activates more than 70 substrates; ranging from chaperones, cytoskeletal and translation machinery, glycolysis proteins to innate immune signaling mediators such as the proinflammatory cytokines; IL-1β and IL-18 [Shao, Yeretssian *et al.*, 2007]. ASC, one of the key components of inflammasomes, is critical to several major inflammatory and cell death-associated signaling pathways (figure 3.1).

Nanoparticles exhibit distinctly varied physico-chemical properties as we move towards the nanoscopic view. Properties of nanoparticles are a function of their size and non-bulk properties of nanoparticles emerge only in particles of diameters less than 20nm [Auffan, Rose *et al.*, 2009]. Nanoparticles have a very large surface-to-volume ratio, so that even small amounts of particles present extremely large surface areas available for protein binding [Cedervall, Lynch *et al.*, 2007]. While some studies report no toxicity of amorphous nanosilica there are several studies supporting the toxic effects of amorphous nanosilica [Li, Sun *et al.*, 2011; Nabeshi, Yoshikawa *et al.*, 2011; Nabeshi, Yoshikawa *et al.*, 2011]. However, clear mechanistic insights with respect to amorphous nanosilica induced inflammation and regulation of immune responses remain undiscovered.

3.3 MATERIALS AND METHODS

3.3.1 Characterization of Amorphous Silica Nanoparticles

The silica nanoparticles used in this study are Ludox® colloidal silica nanoparticles, TM-40 (420786) and HS-40 (420816) available from Sigma. These are monodispersed amorphous silica nanoparticles suspended in H_2O. For Transmission Electron Microscopy, 10µL solution of Ludox® silica was deposited on carbon-coated copper grids. The samples were imaged using FEI Tecnai™ transmission electron microscope (T 20 S-twin, FEI) at the Materials Research Centre facility of Malaviya National Institute of Technology (MNIT), Jaipur.

3.3.2 Cell Culture

A-549 (Sigma-Aldrich, 86012804), human lung carcinoma cell line and CHO (Himedia, CCK005) fibroblasts were grown on Dulbecco's modified eagle medium (DMEM), (Himedia, AL007S) with 10% Fetal bovine serum (Himedia, RM10432) and 1% antibiotic antimycotic solution (Sigma-Aldrich, A5955). Cells were cultured as per company instructions in humidified CO_2 incubators. To simulate inflammation, cells were pre-stimulated with Lipopolysaccharide (LPS; Sigma, L4391). For cell culture experiments, silica nanoparticles were diluted, re-suspended in freshly prepared DMEM-serum free medium and vortexed just before use. For phagocytosis inhibition, cells were pre-treated with 10µM Cytochalasin-D (Cyto-D) for 20 minutes (Sigma, T6025).

3.3.3 Glyburide or Ac-YVAD-cmk Treatment of Cells

Human embryonic kidney (HEK293T) fibroblasts were treated with 0.5µg/mL LPS overnight in DMEM complete growth medium. After LPS priming, medium was aspirated and cells were washed with DMEM-serum free media and 200µL of DMEM-serum free media was added per well in a 96 well plate. Cells were pre-treated with Glyburide – NLRP3 inhibitor (50µM; G0639-5G, Sigma) or Ac-YVAD-cmk – Caspase-1 inhibitor (50µM; SML0429-1MG, Sigma) for 30 minutes before the addition of nanosilica (200µg/mL, 60 minutes). Each experiment was carried out with internal duplicates and every experiment was repeated thrice.

3.3.4 MTT Assay

After exposure to nanosilica (12nm, HS-40/22nm, TM-40), the cytotoxicity caused was assessed by the MTT assay. Nanosilica-containing DMEM-serum free media was removed carefully from the microplate. 100µl of fresh serum free media and 10µl of MTT solution (M2128, Sigma) was added to each well. The plate was kept in incubator (Model-170S, Eppendorf) at 37ºC with 5% CO_2 in dark for 3 hours. After incubation, 100µl of acid/alcohol solution was added to each well. Absorbance was measured at 570nm using multi-mode microplate reader (Synergy H1 Hybrid, Biotek Instruments Inc).

3.3.5 Cytokine measurements: To assess the local levels of IL1β, IL18, and TNF, fresh cell free supernatants were harvested from the silica treated microglial cells and immediately analysed using Human IL-1β/ IL-18/TNF ELISA Set (BD Biosciences) kit.

3.3.6 Bradford assay for protein estimation

For protein extraction, 0.25×10^6 cells were lysed in 0.25 ml RIPA buffer at room temperature for 5 minutes followed by centrifugation at 13,100 rpm for 20 minutes. The supernatants were used for further analyses. Protein concentrations were determined using a coomassie (Bradford) protein assay kit and Nanodrop Spectrophotometer by taking absorbance measured at 595nm.

3.3.7 Fluorescence Microscopy

For immunocytochemistry, we seeded 10^5 cells to each well of a 2-well chamber slide and incubated overnight. Next morning, the cells were treated with 12 and 22nm silica particles (200µg/ml; 60 minutes) and/or Cyto–D (10µM) as per experiment. Treated cells were immunolabeled with anti-ASC/TMS-1 rabbit monoclonal antibody (Cell signaling Technology cat no: 13833S) and Alexa Fluor 594 goat anti-rabbit secondary antibody (Life technologies) and nuclei were counterstained by 4',6-diamidino-2-phenylindole (DAPI, Sigma). Immunofluorescence was observed using fluorescence microscope (Leica Systems) and ImageJ software was used to analyze the images.

3.3.8 Transmission Electron Microscopy

Cells were treated with 200µg/ml of nanosilica (12nm, HS40/22nm, TM40) for 60 minutes. After centrifugation, fixation of the treated cells was carried out by 2.5% glutaraldehyde followed by wash with 1X PBS. The washing step was followed with fixation using 1% Osmium tetroxide. Next, the cells were subjected to dehydration with graded series of alcohol, embedded using an embedding kit, DER 332-732 (EMS, USA) and kept for polymerization for 48 hours. The resultant resin blocks were subjected to ultrathin sectioning using an ultra-microtome (Leica Ultracut UCT, Germany). Each of the 60-70 nm ultrathin section was transferred on Formvar and carbon coated copper grids (EMS, USA) of 300 mesh size. The grids were stained with Uranyl acetate and lead citrate solutions [Schrand, Schlager *et al.*, 2010]. The sections were visualized under Phillips TEM CM 200 at SAIF-IIT Bombay.

3.4 Results and Discussion

3.4.1 Nanosilica induced cytotoxicity in bronchoalveolar epithelial, endothelial and fibroblast cell lines

First, we characterized 12nm and 22nm sized amorphous silica nanoparticles by transmission electron microscopy (Figure 3.2). The 22nm nanosilica (Figure 3.2 (a, b)) showed almost smooth spherical morphology, and the 12nm nanosilica (Figure 3.2 (c, d)) showed spherical morphology with rough surface. The small sized, 12nm nanosilica exhibited high surface area as compared to the large sized, 22nm nanosilica (Table 3.1).

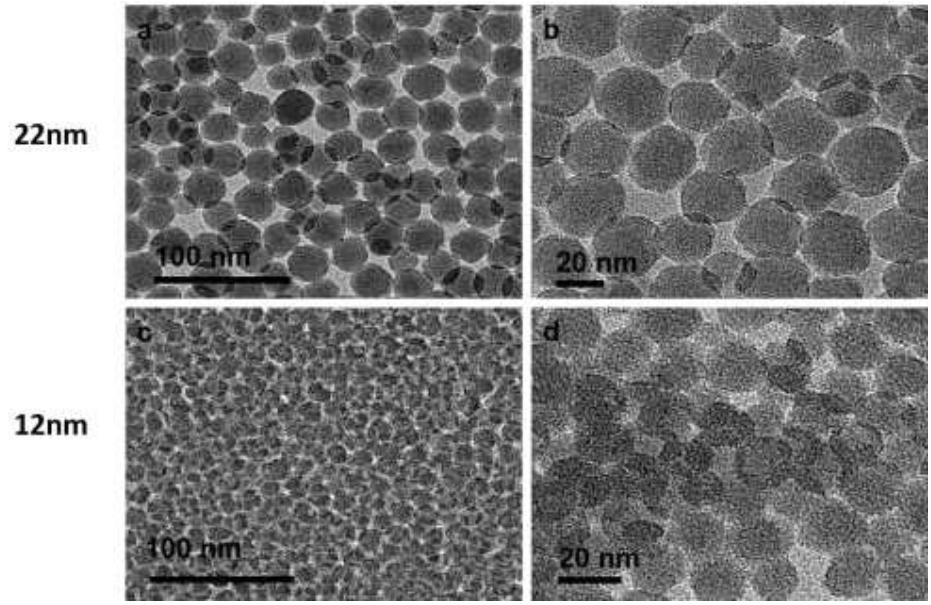

Figure 3.2 : *Characterization of amorphous silica nanoparticles by transmission electron microscopy.* Panel shows, monodispersed 22nm nanosilica (a-b) and 12nm nanosilica (c-d).

Table 3.1 : *Specifications of Amorphous nanosilica*

Silica NP (colloidal)	Molecular weight	Density (g/mL at 25 °C)	Surface area (m^2/g)	Particle Size (nm)	Concentration (percent by weight)	Concentration (mg/ml)
HS-40	60.08	1.3	~220	**~12**	40 wt. % suspension in H_2O	520.29
TM-40	60.08	1.3	~140	**~22**	40 wt. % suspension in H_2O	520.29

The cell-specific effects of nanosilica were investigated using three distinct cell lines representative of lung cell population; bronchoalveolar epithelial, endothelial and fibroblast. To understand irritant exposure duration and time-dependent effects of nanosilica, we exposed cells to varying concentrations of nanosilica ranging from 0, 100, 200, 400 µg/ml, for a time course of 0, 30, 60, 120, and 180 minutes as described in the schematic (Figure 3.3a). Experiments were performed, both in the presence and absence of bacterial LPS to simulate the effect of

preexisting inflammation on the uptake and exposure to nanosilica. The study is focused on characterization of toxic and biological effects of amorphous nanosilica exposure in human lung cell population (Figure 3.3a). Bright field microscopy was performed to visualize morphological changes in cells following nanosilica exposure (Figure 3.3b). The effect of nanosilica on cell morphology and cytotoxicity caused was clearly evident. Interestingly, 12nm nanosilica treated cells showed widespread cell death after 60 minutes of treatment with 200µg/ml concentration as compared to the 22nm nanosilica. However, the 22nm nanosilica treated cells showed several healthy cells even after 60 minutes.

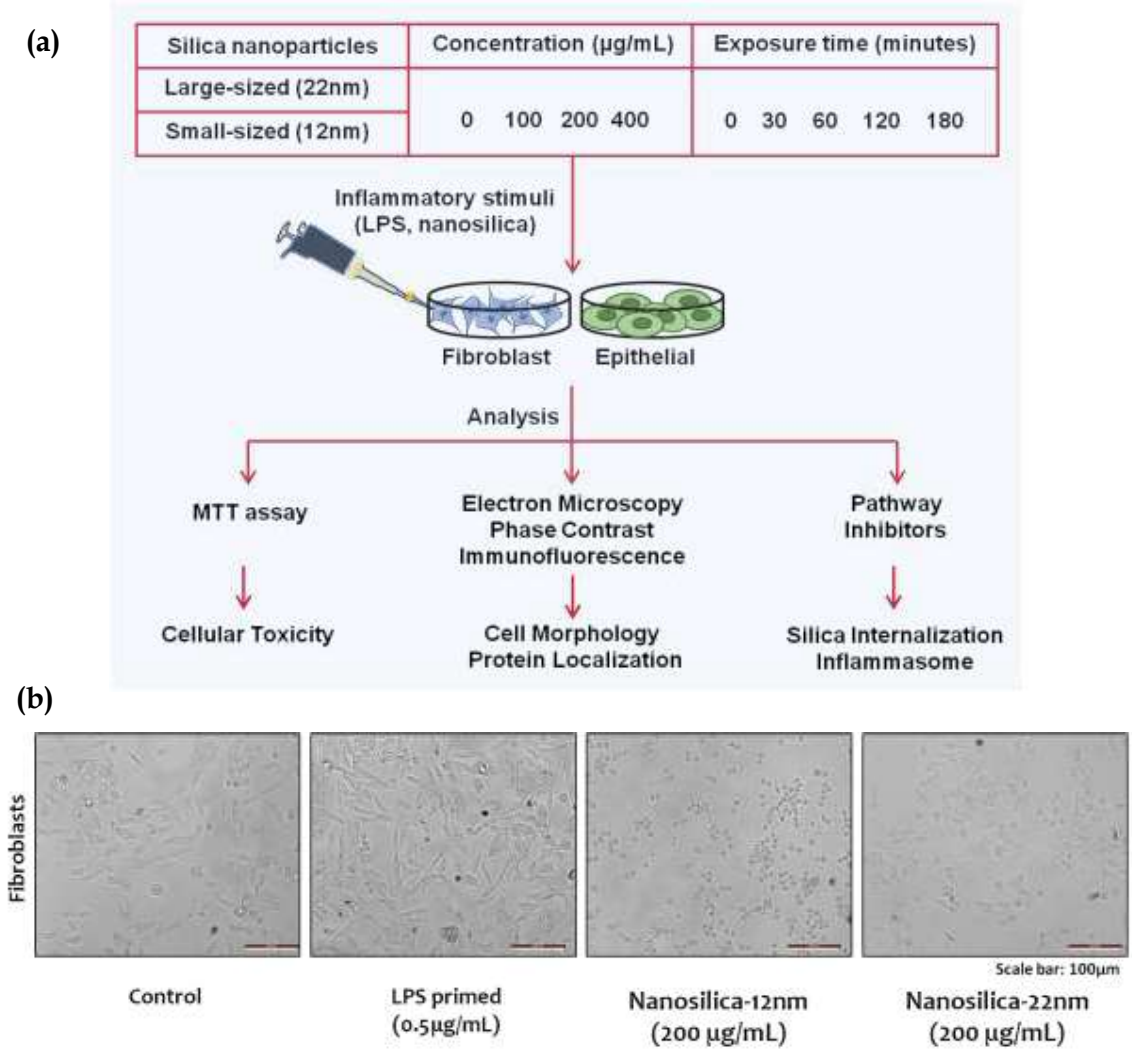

Figure 3.3 : *Schematic for experimental design*. The study analyzes pathways associated with cellular uptake of nanosilica, toxicity mechanisms and mode of cell death in human lung cell population.

3.4.2 Cell specific and size dependent cytotoxic effects of nanosilica

We observed cell specific and nanosilica size dependent differential cytotoxicity for lung cell population. Cytochalasin D (Cyto-D) is a cell-permeable and potent inhibitor of actin polymerization. Cyto-D, an inhibitor of phagocytosis was used to identify actin dependent pathways of uptake within the cells [Schliwa, 1982]. MTT Assay was performed to test for cell viability following nanosilica exposure. To understand the effect of nanosilica exposure in inflammed cells as compared to healthy cells, we used primed cells with LPS to induce

inflammation. Preexisting inflammation induced by LPS did not contribute significantly to cytotoxicity induced by nanosilica. Endothelial cells showed highest sensitivity to cell death in response to 12nm nanosilica followed by epithelial cells. Fibroblast cells were least susceptible to cell death in response to 12nm nanosilica (Figure 3.4a). Interestingly, Cyto-D did not prevent cell death induced by 22nm nanosilica, suggesting a phagocytosis independent pathway for internalization and cytotoxicity in 22 nm nanosilica particles (Figure 3.4b). In case of 12nm nanosilica, cytotoxicity was reduced but not abrogated by Cyto-D treatment suggesting existence of some phagocytosis dependent pathways.

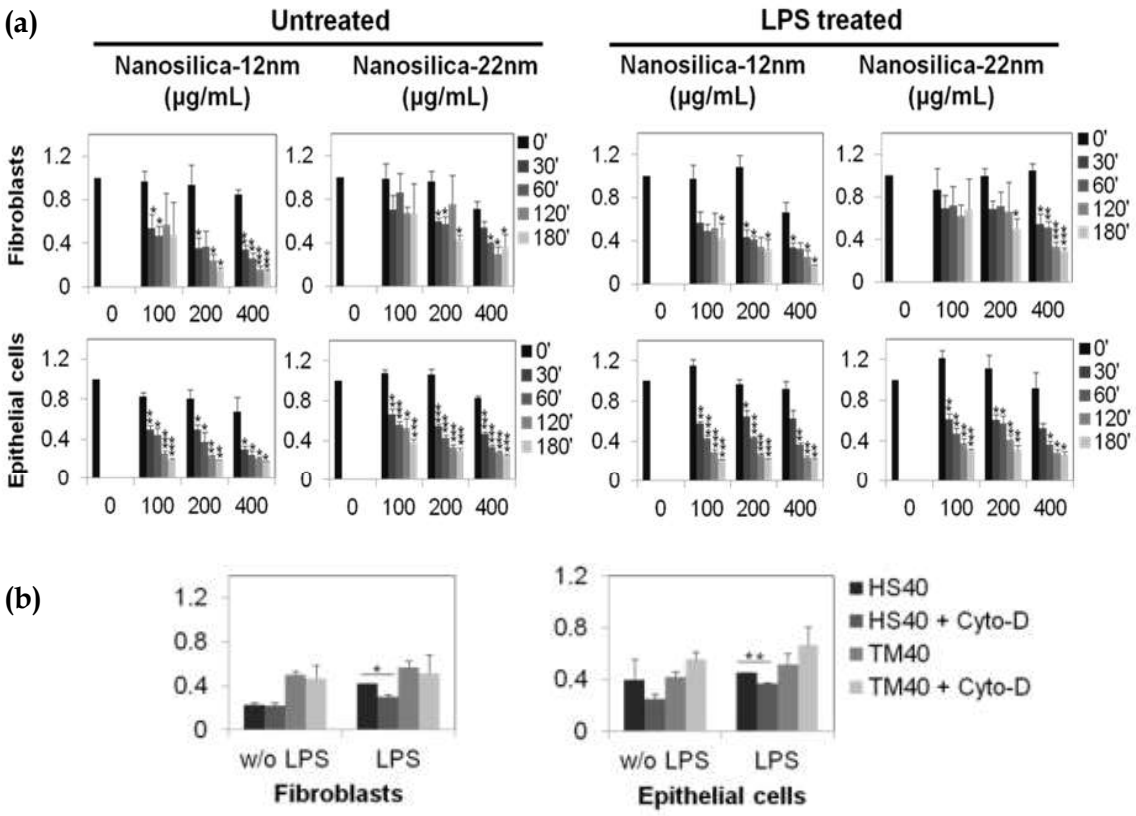

Figure 3.4 : *MTT Assay for assessment of cell viability following nanosilica exposure.* Fibroblast and epithelial cells were left untreated or treated with bacterial LPS (0.5 µg/ml) to simulate inflammation. 12nm and 22nm nanosilica exposure (0, 100, 200 and 400 µg/ml) for 0, 30, 60, 120 and 180 minutes was given to fibroblast and epithelial cells. Fibroblast and epithelial cells were left untreated (w/o LPS) or treated with LPS followed by Cyto-D treatment (10µM, 20 minutes) prior to nanosilica exposure (HS40,12nm/ TM40,22nm; 200µg/ml; 60 minutes). Each experiment had internal duplicates. n=3 for each experiment. Error bars indicate Standard error of mean. *p <0.05, **p<0.005 and ***p<0.0005.

3.4.3 Amorphous nanosilica dependent cytotoxicity is NLRP3 and Caspase-1 independent.

NLRP3 can sense DAMPs such as; changes in ATP concentration, uric acid, amyloid -β, hyaluronan and heparan sulfate, PAMPs such as; bacterial and viral nucleic acids and irritants such as; crystalline silica, asbestos and alum. NLRs associate with the adapter protein ASC and Procaspase-1 to form multi-protein complexes called inflammasomes [Latz, Xiao *et al.*, 2013; Guo, Callaway *et al.*, 2015]. Crystalline silica activates the NLRP3 inflammasome following phagocytosis and rupture of lysosomal membranes leading to release of cathepsin-B [Dostert, Petrilli *et al.*, 2008]. However, similar mechanisms for amorphous nanosilica remain unknown. The type II Diabetes drug, Glyburide is known to inhibit NLRP3 inflammasome activation

[Lamkanfi, Mueller *et al.*, 2009]. Glyburide's cyclohexylurea group, which binds to adenosine triphosphatase (ATP)–sensitive K+ (KATP) channels for insulin secretion, is dispensable for inflammasome inhibition. We utilized glyburide treatment before exposure to 12nm or 22nm nanosilica to evaluate the contribution of NLRP3 dependent pathways in cell death. Interestingly, glyburide treatment did not prevent cell death induced by both 12 and 22nm nanosilica indicating an NLRP3 independent pathway (Figure 3.5 (a-b)). In the inflammasome complex, inactive procaspase-1 undergoes autocatalytic cleavage to form active Caspase-1 [Srinivasula, 2002]. Caspase-1 in turn can cleave and activate more than 70 substrates, ranging from chaperones, cytoskeletal and translation machinery, and glycolysis proteins to immune proteins, such as the proinflammatory cytokines; IL-1β and IL-18 [Shao, Yeretssian *et al.*, 2007; Keller, Rüegg *et al.*, 2008]. Stimuli that induce the activation of Caspase-1 to process cytokines do not necessarily cause cell death[Saleh and Green, 2007]. To investigate caspase-1 dependence of nanosilica cell death we pre-treated cells with Ac-YVAD-cmk, a highly selective, cell-permeable, irreversible Caspase-1 inhibitor, followed by exposure to nanosilica. Ac-YVAD-cmk is a chloromethyl ketone tetrapeptide based on the target sequence in proIL-1β (YVHD). YVAD treatment did not attenuate 12nm and 22nm nanosilica cell death (Figure 3.5 (c-d)).

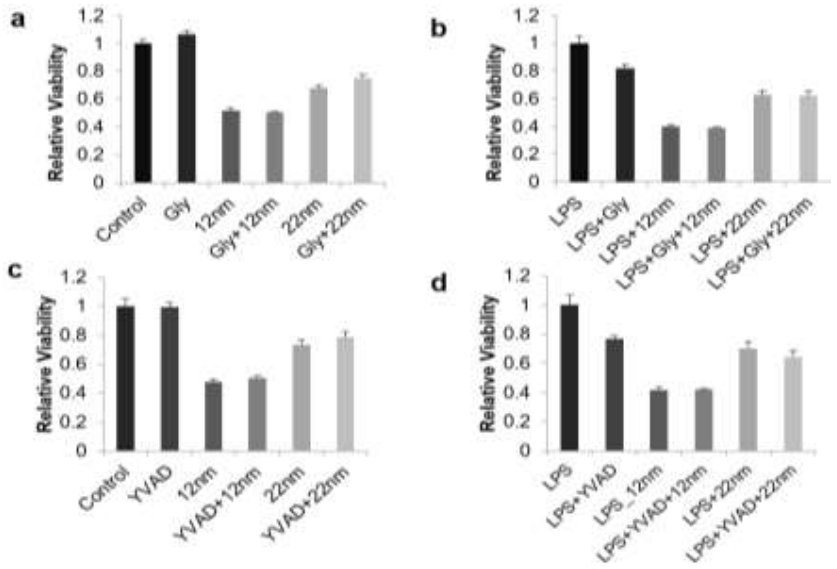

Figure 3.5 : *Amorphous nanosilica dependent cytotoxicity is Caspase-1 and NLRP3 independent.* (a,b) Untreated fibroblasts were pre-treated with the NLRP3 inhibitor, glyburide (50μM) for 30 minutes followed by silica nanoparticles (200μg/mL, 60 minutes). Fibroblasts were primed with LPS overnight and pre-treated with glyburide followed by nanosilica exposure. (c,d) Untreated fibroblasts were pre-treated with the Caspase-1 inhibitor, Ac-YVAD-cmk (50μM) for 30 minutes followed by silica nanoparticles (200μg/mL, 60 minutes). LPS primed fibroblasts were pre-treated with Ac-YVAD-cmk followed by nanosilica exposure. n=3 for each experiment. Each experiment had internal duplicates. Error bars indicate SEM.

3.4.4 Amorphous nanosilica induces increase in ASC expression

To further investigate the underlying mechanism of amorphous nanosilica induced cell death we utilized fluorescence microscopy to investigate the cytoplasmic expression of the inflammasome adapter protein ASC in bronchoalveolar epithelial, endothelial and fibroblast cell lines. ASC is central to several inflammatory and cell death pathways in innate and adaptive immune responses. ASC is essential for LPS-induced activation of Procaspase-1 independently of TLR-associated signal adaptor molecules [Yamamoto, Yaginuma *et al.*, 2004] . In figure 3.6, immunofluorescence for ASC revealed that while, both 12 and 22nm nanosilica

exposure caused an increase in ASC expression, the intracellular localization was different. 12nm nanosilica caused the cells to have punctate expression of ASC specks, while 22nm nanosilica caused cells to have diffuse cytoplasmic expression (Figure 3.6 (a, b)). To further characterize intracellular localization of ASC we utilized confocal microscopy.

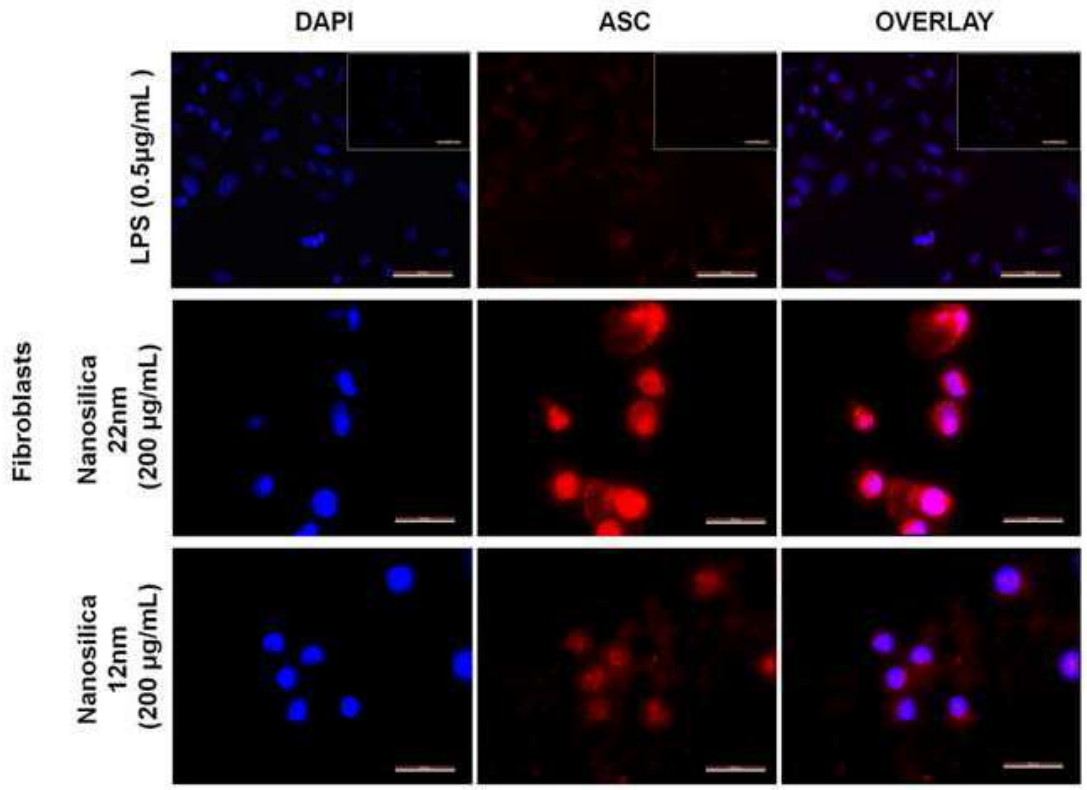

Figure 3.6 : *ASC expression in nanosilica treated cells was analysed by immunofluorescence.* Anti-ASC antibody was used to stain ASC (red). DAPI was used to stain nuclei (blue). a) In untreated fibroblast cells ASC staining is diffuse and cytoplasmic. In 22nm nanosilica treated cells ASC expression increases with intense cytoplasmic as well as perinuclear staining. In 12nm nanosilica treated fibroblast cells the staining is punctate showing distinct specks throughout the cytoplasm and nucleus. Scale bar is 50µm.

3.4.5 Amorphous nanosilica induces nuclear ASC speck formation

LPS induces formation of ASC supramolecular assembly referred to as apoptotic speck or pyroptosome [Fernandes-Alnemri, Wu *et al.*, 2007]. In bone marrow derived macrophages, ASC speck formation is required for processing of IL-1β but dispensable for pyroptosis induction. Oligomerization of ASC creates several Caspase-1 activation sites resulting in signal amplification for inflammasome dependent cytokine production [Lu, Magupalli *et al.*, 2014]. Confocal microscopy utilizing an anti- ASC antibody showed that cytoplasmic and diffuse expression of ASC in untreated cells increases upon LPS stimulation (Figure 3.7a). Following 12nm nanosilica exposure cells showed nuclear condensation and presence of perinuclear and nuclear ASC specks. In contrast, 22nm nanosilica exposure resulted in perinuclear and diffused nuclear localization. Quantification of specks confirms an increase in apoptotic specks in 22nm nanosilica treated cells as compared to 12nm nanosilica treated cells (Figure 3.7b). We also observed significant decrease in ASC speck count per cell, upon pre-treatment of Cyto-D before silica exposure. The inhibition effect of Cyto-D on ASC speck formation was statistically significant against 12nm as well as 22nm silica exposure (UT vs. LPS (*p-value= 0.04); LPS vs.

LPS- 22nm nanosilica (**p-value= 0.004); LPS- 12nm vs. LPS- Cyto-D- 12nm (*p-value= 0.02); LPS- 22nm vs. LPS- Cyto-D- 22nm (*p-value= 0.04).

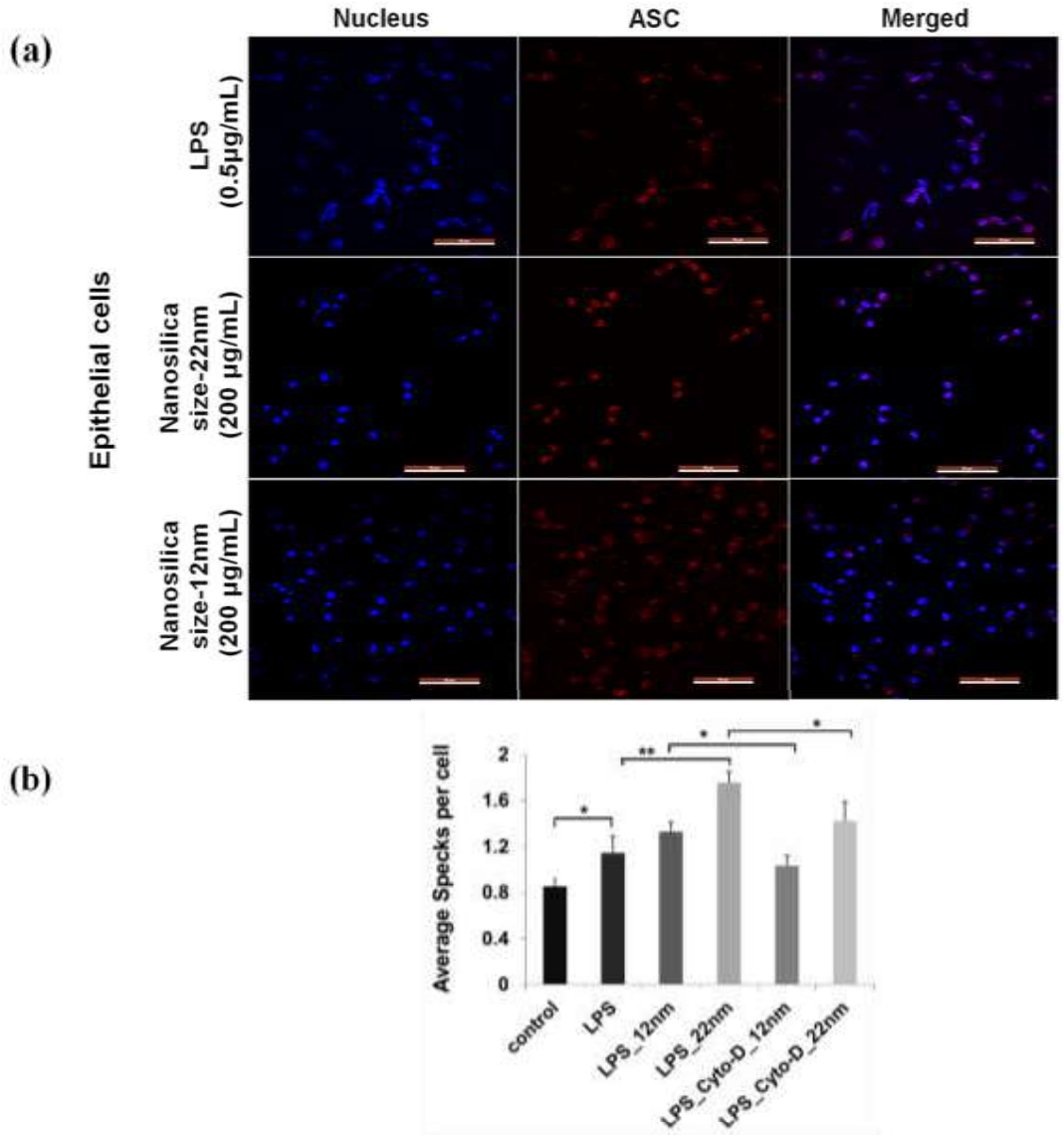

Figure 3.7 : *Confocal microscopy for ASC speck quantification in epithelial cells.* (a) Anti-ASC antibody was used to stain ASC red. DAPI was used to stain nuclei blue. In 12nm treated cells nuclear specks are seen while in 22nm nanosilica treated cells both nuclear ASC specks and perinuclear staining is observed. Quantification of average number of specks per cell shows a significant increase following nanosilica exposure (b). There is a significant decrease in number of specks following cytochalasin-D treatment. Error bars indicate SEM. P-values - *p <0.05, **p<0.005, ***p<0.0005. Scale bar is 100 µm.

3.4.6 Size dependent distinct cell death pathways induced by nanosilica

Morphological changes in cell shape following 12 and 22nm nanosilica treatment, visualized by bright field microscopy suggested distinct cell death pathways. We utilized transmission electron microscopy to further investigate the cell-death pathways associated with nanosilica induced cell death. We found that cells treated with 12nm nanosilica (Figure 3.8) showed characteristic necrotic cell death while 22nm nanosilica suggested apoptotic cell death. In case of the necrotic cells a swollen cytoplasm, disruption of the plasma membrane and organelles is discernible while in the apoptotic cells the nucleus is condensed, the cell is

shrunken in size and cellular blebbing is evident [Fink and Cookson, 2005; Bortner and Cidlowski, 2014] .

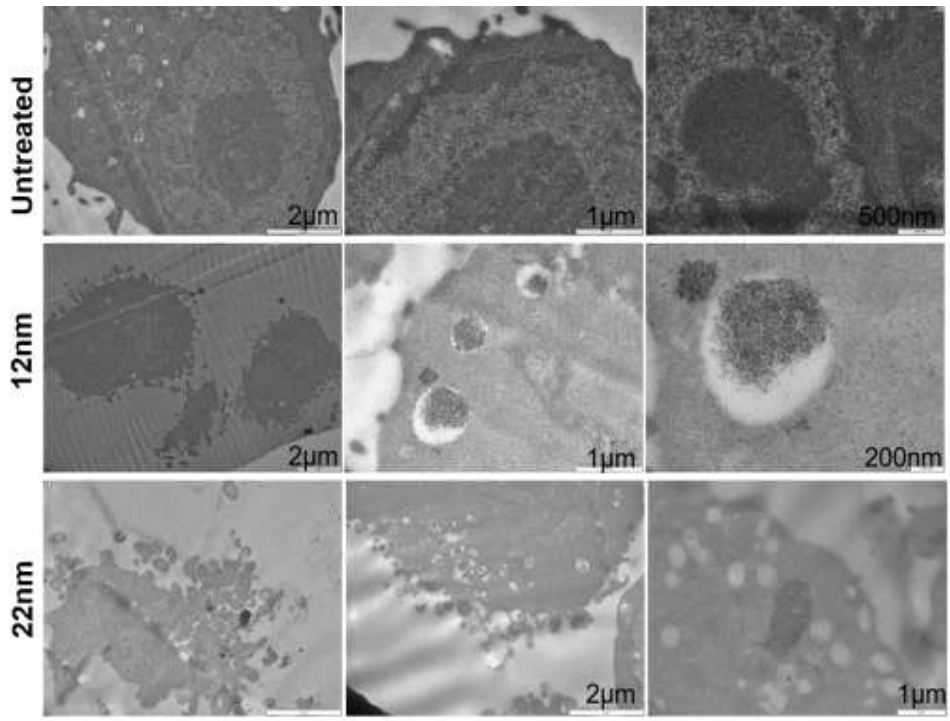

Figure 3.8 : *Characterization of nanosilica internalization and subsequent cell death.* Transmission electron microscopy of 12nm treated cells show characteristic necrotic morphology while 22nm treated cells appear apoptotic.

3.4.7 Inflammatory cytokines release in nanosilica treated microglia

Previous studies have shown cell specific inflammation responses and cytokine release in response to different sized nanosilica particles [Shirasuna, Usui *et al.*, 2015; Låg, Skuland *et al.*, 2018]. To better understand the role of inflammasome and major inflammation-associated pathways, ELISA was performed for measuring the change in IL-1β, IL-6 and TNF cytokines synthesis and release in nanosilica treated cells (Figure 3.9). Results demonstrate significant increase in IL-6 and TNF release, when exposed to both 12 and 22nm nanosilica. We also observed significant IL-6 increase and IL-1β decrease, specifically in 12nm nanosilica treated macrophages. However, IL-1β levels remain same in both control and nanosilica exposed microglia and macrophages, suggesting NLRP3 and NLRC4-independent inflammation pathways induction in response to nanosilica.

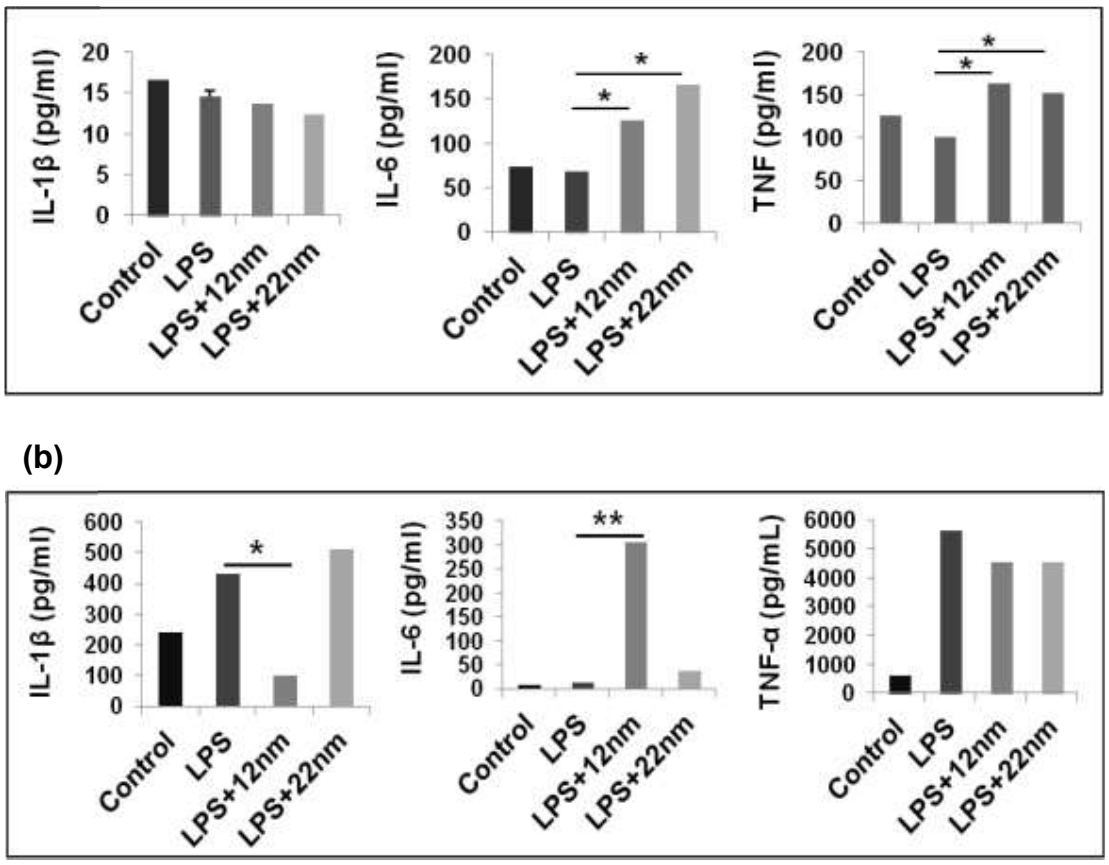

Figure 3.9 : *Cytokines expression analysis in response to silica exposure.* We performed ELISA to measure IL-1β, IL-6 and TNF release in nanosilica (HS40-12nm/TM40-22nm; 60 minutes) treated BV2 microglia and PMA treated THP-1 macrophages. (a) IL-1β levels remained almost same for control (untreated) and nanosilica-treated microglia. Significant increase in IL-6 and TNF levels was observed for both 12 and 22nm nanosilica exposure. (b) TNF levels remained same for control (untreated) and nanosilica-treated THP-1 macrophages. Interestingly, IL-6 increased and IL-1β decreased specifically for cells treated with 12nm sized silica.

3.5 CONCLUDING REMARKS

NLRs are important cellular platforms for effective regulation of inflammatory and innate immune responses, generated against several endogenous and exogenous damage- and pathogen-associated stimuli and irritants. Crystalline silica, one of the most common and potent NLR-activating ligand, has been linked to several inflammation associated pulmonary dysfunctions and cancer. Interestingly, amorphous nanosilica holds high commercial value and advanced biomedical applications because of its inert and non-toxic behavior. Despite its widespread use, amorphous nanosilica-mediated cellular and molecular interactions with the human biological system, dysregulated immune responses and its long term effects are not well-studied [Shirasuna, Usui *et al.*, 2015; Tarantini, Lanceleur *et al.*, 2015]. As known already, the most common route of nanosilica entry into humans is through lungs. Therefore, this study focuses on the cellular and molecular effects of amorphous nanosilica in human lung cell population. We observed both time and concentration dependent increase in nanosilica induced toxicity in different lung cell types. Different cell types showed different susceptibility to nanosilica induced cytotoxicity. The endothelial cells were highly sensitive to nanosilica exposure, followed by the epithelial and fibroblasts cell lines. ASC expression and speck formation increases in response to 12nm nanosilica. Also, specific nuclear translocation of ASC occurs during 12nm nanosilica-induced inflammation. Interestingly, small-sized (12nm) nanosilica was more cytotoxic as compared to the large-sized (22nm) nanosilica. While, 22nm nanosilica treated cells underwent apoptosis, the 12nm nanosilica exposure lead to necrosis. In fact, the cellular uptake is actin cytoskeleton dependent in 22nm and independent for the 12nm sized nanosilica. Based on these findings, we suggest that the differential cytotoxic and inflammatory effects of amorphous nanosilica must be kept under consideration while using amorphous nanosilica for various biomedical and, industrial applications.